

Periodic tidal loading reveals stress dependence of the earthquake size distribution (b value)

Yen Joe Tan¹, Felix Waldhauser¹, Maya Tolstoy¹, and William S. D. Wilcock²

¹Lamont-Doherty Earth Observatory of Columbia University, Palisades, New York 10964, USA.

²School of Oceanography, University of Washington, Seattle, WA 98195, USA.

Key Points:

- The earthquake b value decreases with increasing tidal stress.
- b values can be used to map stress variations in the Earth's crust.

arXiv:1810.04333v1 [physics.geo-ph] 10 Oct 2018

Corresponding author: Yen Joe Tan, yjt@ldeo.columbia.edu

Abstract

Earthquake size-frequency distribution follows a power law, with the b value often used to quantify the relative proportion of small and large events. Laboratory experiments have found that the b value of microfractures decreases with increasing stress. Studies have inferred that this relationship also holds for earthquakes based on observations of earthquake b values varying systematically with faulting style, depth, and subducting plate age. However, these studies are limited by small sample sizes despite aggregating events over large regions, which precludes the ability to control for other variables that might also affect earthquake b values such as rock heterogeneity and fault roughness. Our natural experiment in a unique seafloor laboratory on Axial Seamount involves analyzing the size distribution of $\sim 60,000$ earthquakes which delineate a ring-fault system in a 25 km^3 block of crust that experiences periodic tidal loading of $\pm 20 \text{ kPa}$. We find that the b value decreases with increasing tidal stress. Our result increases the confidence in using b values to estimate stress variations in fault zones through their seismic cycles, which can help improve forecasting of large earthquakes.

1 Introduction

Earthquake occurrences are primarily controlled by the stress state on fault interfaces. Since *in situ* stress measurements are difficult to obtain, having a proxy for estimating the stress state of fault zones through their seismic cycles is critical for earthquake forecasting. Earthquakes follow a power law size-frequency distribution given as $\log_{10}(N) = a - bM$, where N is the number of earthquakes greater than or equal to magnitude M , and a and b are the constants [Gutenberg and Richter, 1944]. The value a describes the total number of earthquakes while the b value describes the relative frequency of small and large magnitude earthquakes. In rock fracture experiments, acoustic emissions from small cracking events follow the same power law size distribution [Scholz, 1968]. Furthermore, their b values have been found to decrease (larger proportion of large events) with increasing stress [Scholz, 1968; Amitrano, 2003; Goebel *et al.*, 2013].

The same stress dependence of b value has been inferred to apply to earthquakes. The b value of earthquakes has been found to vary systematically with faulting style [Schorlemmer *et al.*, 2005], depth [Spada *et al.*, 2013], and for subduction zone earthquakes, plate age [Nishikawa and Ide, 2014]. These observations are consistent with the earthquake b value decreasing with increasing differential stress [Scholz, 2015]. However, these studies were

restricted to using minimum bins of as few as 50 to 200 earthquakes to calculate the b values, which is barely a large enough sample size to even establish the existence of a power law distribution [Stumpf and Porter, 2012]. In addition, these studies had to aggregate events over large regions and thus were unable to control for other variables that might also affect earthquake b values such as rock heterogeneity [Mori, J. and Abercrombie, R. E., 1997] and fault roughness [Goebel, T. H. et al., 2017]. Establishing whether earthquake b value varies systematically with stress is critical for demonstrating its potential as a stress meter in the Earth's crust which can help improve forecasting of large earthquakes [Schorlemmer and Wiemer, 2005; Nanjo et al., 2012; Gulia et al., 2016].

Axial Seamount is formed at the intersection of the Juan de Fuca Ridge and the Cobb-Eickelberg hotspot. As part of the Ocean Observatory Initiative (OOI), a cabled seismic network was installed on the summit of the volcano (Fig. 1a) with time-corrected seismic data streaming from late January 2015 [Wilcock et al., 2016]. In the three months before the volcano erupted in April 2015, ~60,000 earthquakes were located using the double-difference method [Waldhauser and Ellsworth, 2000] and delineate an outward-dipping ring-fault system that extends to ~2-km depth [Wilcock et al., 2016] (Fig. 1). The large number of events located within a small region, combined with the earthquakes' sensitivity to tidal stress perturbations [Wilcock et al., 2016], make this the perfect natural laboratory to test how the earthquake b value relates to stress changes.

2 Methods

2.1 Earthquake Catalog

In the first year of operation, ~70,000 earthquakes were located by the OOI Axial seismic network [Wilcock et al., 2016]. In the three months before the volcano erupted, the majority of the composite focal mechanisms determined showed normal or oblique-normal sense of motion. During the one-month-long eruption period, the slip direction was reversed as the volcano deflated [Levy et al., 2018]. After the eruption, the seismicity rate decreased substantially [Wilcock et al., 2016, 2018] with the focal mechanisms suggesting heterogeneous fault slip directions [Levy et al., 2018]. Therefore, in this paper, we only examine the ~60,000 earthquakes that occurred in the three months before the volcano erupted. The earthquake catalog, including the moment magnitudes (M_W) estimated following Tréhu and Solomon [1983], has been previously published [Wilcock et al., 2016].

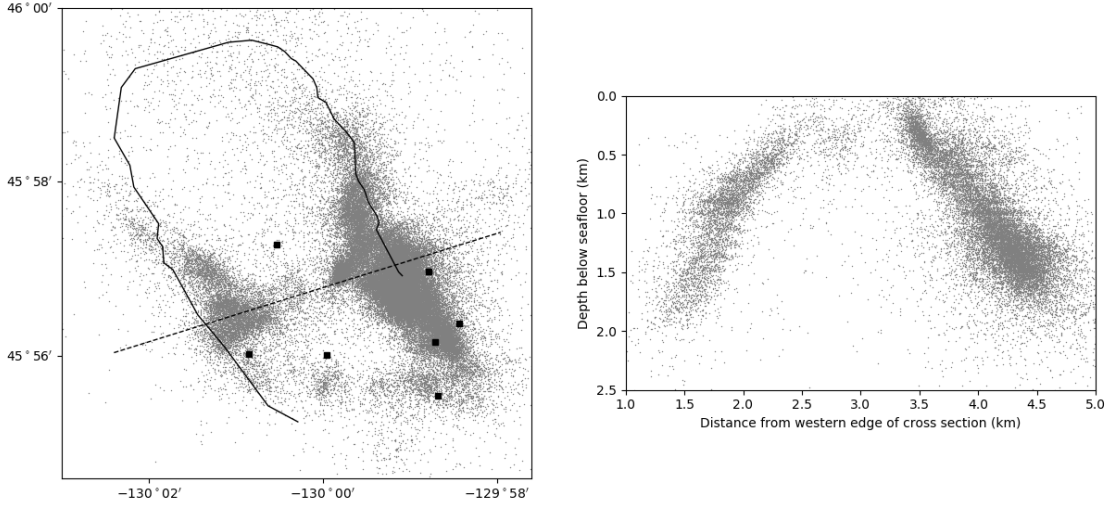


Figure 1. Locations of earthquakes above M_c . **a.** Earthquake epicenters (grey dots), seismometers (black filled squares), caldera rim (black line), and the cross section shown in (b) (black dashed line). **b.** Depth cross-section across the caldera showing the projected earthquake locations within 0.5 km of the profile.

We first estimate the magnitude of completeness (M_c) of the catalog using the point of maximum curvature of the frequency-magnitude distribution (FMD) [Wiemer and Katsumata, 1999], which is equivalent to finding the magnitude bin with the highest number of earthquakes in the non-cumulative FMD [Mignan and Woessner, 2012]. We find $M_c = 0.0$. We then estimate M_c using the goodness-of-fit (GFT) method by comparing observed and synthetic FMDs [Wiemer and Wyss, 2000]. We calculate synthetic FMDs using estimated a and b values of the observed earthquake catalog assuming a range of increasing cutoff magnitudes M_{co} . The goodness-of-fit is quantified using the parameter R :

$$R_{M_{co}} = 100 - \left(100 \frac{\sum_{M_{co}}^{M_{max}} |O_i - S_i|}{\sum_{M_{co}}^{M_{max}} O_i} \right), \quad (1)$$

where O_i and S_i are the observed and predicted number of earthquakes in each magnitude bin. M_c is then the first M_{co} where R has $\geq 90\%$ fit [Wiemer and Wyss, 2000]. We find $M_c = 0.1$. Since the maximum curvature method can underestimate M_c [Wiemer and Wyss,

2000], we decide to use $M_c = 0.1$ as estimated using the GFT method, which leaves us with $\sim 35,000$ earthquakes above M_c .

2.2 Tidal Stress

We estimate the horizontal strains due to body tides using the SPOTL software [Agnew, 1997]. We then calculate the vertical strain from the horizontal strains assuming a plane stress condition

$$\Delta\tau_{zz} = \frac{-\nu}{1-\nu}(\Delta\tau_{xx} + \Delta\tau_{yy}), \quad (2)$$

using Poisson's ratio ν of 0.23. For the effects of ocean tidal loading, we first obtain the predicted tidal height for the eight major short-period tidal constituents (K1, K2, M2, N2, O1, P1, Q1, and S2) using the EOT11a global ocean tidal model [Savcenko and Bosch, 2012] combined with the Oregon State University regional ocean tidal model for the west coast of the United States [Egbert and Erofeeva, 2002] as provided with the SPOTL software. We then estimate the horizontal strains due to variable regional ocean tidal loading using the SPOTL software, which uses a mass-loading Green's function for strain based on the Gutenberg-Bullen Earth model [Agnew, 1997]. We calculate the vertical strain from the horizontal strains assuming a plane stress condition before converting strains to stresses using elastic constants consistent with $V_P = 5.4$ km/s, $V_S = 3.2$ km/s, and a density of 2800 kg/m³. Finally, we estimate the vertical stress perturbation due to direct ocean tidal loading as

$$\Delta\sigma_{zz} = \rho gh, \quad (3)$$

where ρ is the density of seawater (1030 kg/m³), g is the gravitational acceleration (9.8 m/s²), and h is the tidal height relative to its mean value. We then estimate the horizontal stresses from the vertical stress assuming uniaxial strain

$$\Delta\sigma_{xx} = \Delta\sigma_{yy} = \frac{\nu}{1-\nu}\Delta\sigma_{zz}, \quad (4)$$

We combine all the different components of tidal stress to form the stress tensor. We calculate the tidal-stress time series in 5-minute intervals. We assume the stresses estimated at the seafloor applies to the earthquake source region because the tidal wavelengths are very long compared to the earthquake depths of mostly < 2 km (Fig. 1b).

We assume the earthquakes are predominantly normal faulting and/or crack-opening events since the ring-fault system was inferred to have accommodated pre-eruptive inflation [Wilcock *et al.*, 2016], 31 of the 39 (79%) composite focal mechanisms determined before

the eruption based on first-motion polarity showed normal or oblique-normal sense of motion [Levy *et al.*, 2018], and this is a region of tectonic extension. Therefore, we focus on variations in volumetric stress (trace of the stress tensor) due to the combined effects of ocean loading and body tides, with tensional stresses being positive. The tidal stresses have estimated amplitudes of ± 20 kPa (Fig. S1).

2.3 b Value

We estimate the b values using the maximum likelihood method [Aki, 1965], accounting for the use of binned magnitudes [Utsu, 1966]:

$$b = \frac{\log_{10} e}{\bar{M} - \left(M_c - \frac{\Delta M}{2} \right)}, \quad (5)$$

where M_c is the magnitude of completeness of the data set, \bar{M} is the mean magnitude of earthquakes with magnitude $\geq M_c$, and ΔM is the binning interval of the magnitude, which is 0.1 in this study. We estimate the standard deviation of the b value estimate following *Shi and Bolt* [1982]:

$$\delta b = 2.3b^2 \sqrt{\frac{\sum_i^n (M_i - \bar{M})^2}{n(n-1)}}, \quad (6)$$

where n is the sample size. We quantify the significance of the b value difference between two groups of earthquakes using Utsu's test [Utsu, 1999]:

$$p \approx \exp\left(\frac{-\Delta AIC}{2} - 2\right), \quad (7)$$

$$\Delta AIC = -2(N_1 + N_2) \ln(N_1 + N_2) + 2N_1 \ln\left(N_1 + \frac{N_2 b_1}{b_2}\right) + 2N_2 \ln\left(N_2 + \frac{N_1 b_2}{b_1}\right) - 2, \quad (8)$$

where p is the probability that the two groups of earthquakes are drawn from the same population, AIC is the Akaike's information criterion, N_1 and N_2 are the number of earthquakes, and b_1 and b_2 are the estimated b values of the two groups of earthquakes.

3 Results

Using the whole catalog, we obtain a b value of 1.31 ± 0.01 . This is consistent with previous observations of b value > 1 for normal fault events [Schorlemmer *et al.*, 2005] and in marine volcanic environments [Bohnenstiehl *et al.*, 2008]. We assign each earthquake a tidal stress value based on their origin time relative to the tidal stress time series. We find that the seismicity rate increases systematically with increasing tidal volumetric tensional

stresses (Fig. S2), consistent with previous studies at Axial Seamount [Tolstoy *et al.*, 2002; Wilcock *et al.*, 2016] and other mid-ocean ridge environments [Wilcock, 2001; Stroup *et al.*, 2007; Tan *et al.*, 2018].

After sorting the earthquakes based on their associated tidal stress values, we calculate the b values for moving bins of 10,000 events, shifted by 5,000 events. For each bin, we recalculate M_c and find that M_c remains constant at 0.1. The earthquake b value decreases linearly with increasing tidal volumetric stress (Fig. 2). We observe the same trend when using non-overlapping bins of 5,000 events (Fig. S3) and 2,500 events (Fig. S4). This inverse relationship between b value and tidal volumetric stress is clearer for stress amplitude > 0 kPa (Fig. 2, Figs S3 and S4). The larger scatter at smaller stress amplitudes is probably because we have to group events over greater stress ranges for b value estimates as seismicity rate decreases with decreasing stress (Fig. S2).

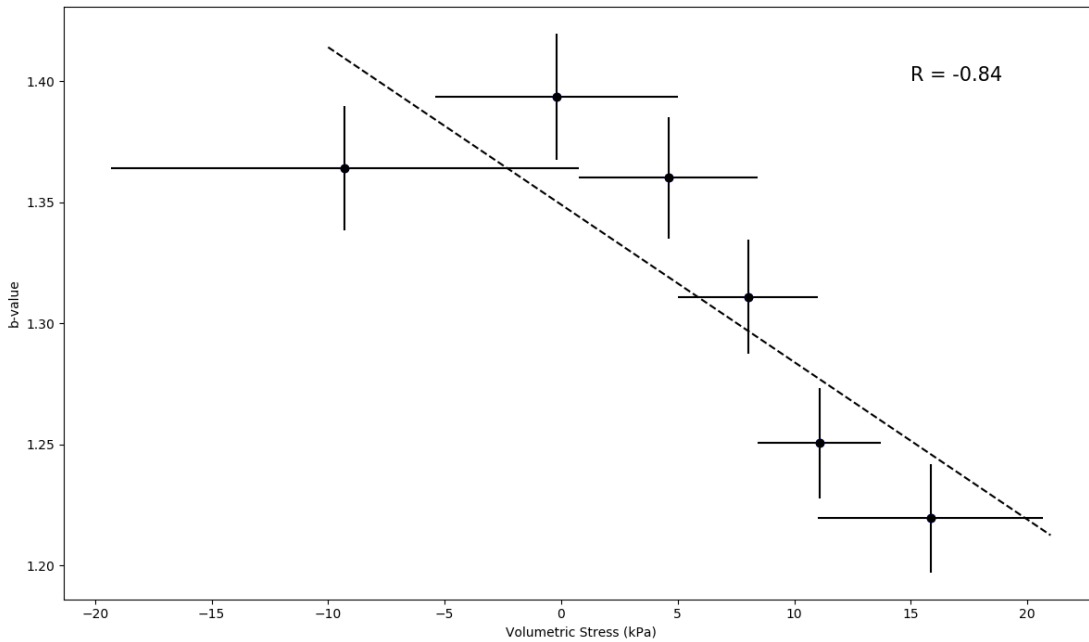


Figure 2. The earthquake b values as a function of tidal stress in bins of 10,000 earthquakes, shifted by 5,000 events. The vertical error bars represent two standard deviations of the estimated b values. The horizontal bars represent the range of earthquake tidal stress values included in each bin. $b = 1.35 \pm 0.03 - (0.007 \pm 0.003)\sigma$ where stress is in kPa.

We further analyzed the frequency-magnitude distribution (FMD) of two separate groups of earthquakes: 10,000 earthquakes occurring during times of largest tidal stresses and 10,000 earthquakes occurring during times of smallest tidal stresses. The slope of the FMD curve for the low tidal stress group is consistently steeper (larger b value) than that of the high tidal stress group, as reflected by the separation of the two curves for the whole magnitude range (Fig. 3). The low tidal stress group has a b value of 1.364 ± 0.013 while the high tidal stress group has a b value of 1.220 ± 0.011 . The b value difference between the two groups is statistically significant at a $> 99\%$ level based on the Utsu's test [Utsu, 1999]. We test the robustness of our result by arbitrarily assuming a higher M_c of 0.5. This leaves us with $\sim 10,000$ earthquakes above M_c . We split the earthquakes into two groups: 5,000 earthquakes occurring during times of largest tidal stresses and 5,000 earthquakes occurring during times of smallest tidal stresses. The low tidal stress group has a b value of 1.451 ± 0.020 while the high tidal stress group has a b value of 1.358 ± 0.018 (Fig. 4). The b value difference between the two groups remains statistically significant at a $> 99\%$ level based on the Utsu's test [Utsu, 1999].

We further verified that the minimum bin sizes often used to document b value variations [Schorlemmer *et al.*, 2005; Spada *et al.*, 2013; Nishikawa and Ide, 2014] are insufficient to robustly constrain our observed effect. We determine the minimum bin size needed to resolve the b value differences we observe as follow: For a range of bin sizes, we calculate 1,000 b values using events randomly drawn without replacement from the original population. Events are drawn from two populations of earthquakes: 10,000 earthquakes occurring during times of largest tidal stresses and 10,000 earthquakes occurring during times of smallest tidal stresses (see Fig. 3). We find that a minimum bin size of 1,100 is needed for the b value distributions of the two populations of earthquakes to not overlap over two standard deviations (Figure 5).

In multiple continental regions, earthquake b values have been found to decrease with increasing depth which has been interpreted to be a result of increasing crustal strength [Spada *et al.*, 2013] and material homogeneity [Mori, J. and Abercrombie, R. E., 1997] with depth. We similarly find that at Axial Seamount, earthquake b values decrease with increasing depth (Fig. S5). Therefore, if there are more deeper earthquakes with increasing tidal volumetric stress, this could explain our observations. However, the earthquake depth distributions of the low and high tidal stress groups are very similar (Fig. S6) with a difference in mean depths of only ~ 11 m and median depths of only ~ 17 m. In addition, the slight change in

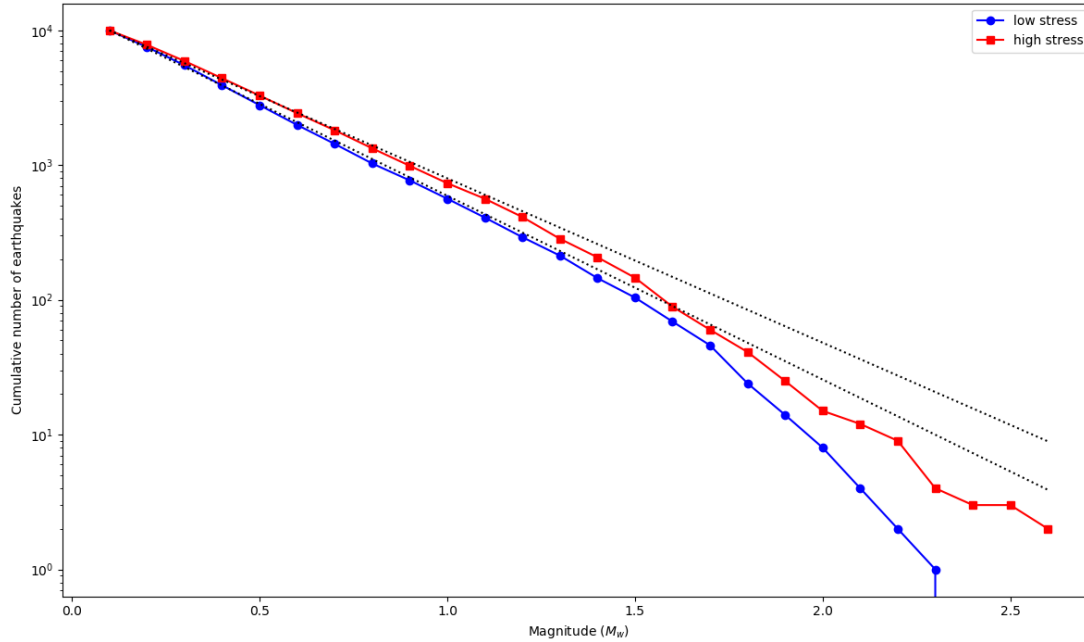


Figure 3. Cumulative frequency-magnitude distributions (FMDs) of two groups of earthquakes: 10,000 earthquakes occurring during times of largest tidal stresses and 10,000 earthquakes occurring during times of smallest tidal stresses. The slope of the cumulative FMD of the low tidal stress group is consistently steeper (larger b value) than that of the high tidal stress group. Dotted lines indicate maximum likelihood fits to the data. The low tidal stress group has a b value of 1.364 ± 0.013 while the high tidal stress group has a b value of 1.220 ± 0.011 .

depth distribution is such that there are slightly more deeper earthquakes for the low tidal stress group. Therefore, our observation of earthquake b value decreasing with increasing tidal volumetric stress is unlikely to be a secondary effect of change in earthquake depth distribution with tides.

A previous study calibrated the stress dependence of earthquake b values assuming a simple frictional strength model combined with measurements of b value variation with depth at different tectonic environments [Spada *et al.*, 2013] and found that b values vary by $\sim 0.001 \text{ MPa}^{-1}$ [Scholz, 2015]. However, our analysis suggests that earthquake b values at Axial Seamount vary by $\sim 7 \text{ MPa}^{-1}$ (Fig. 2, Figs S3 and S4). Laboratory experiments previously showed that b value variations depend on stress normalized to the maximum fail-

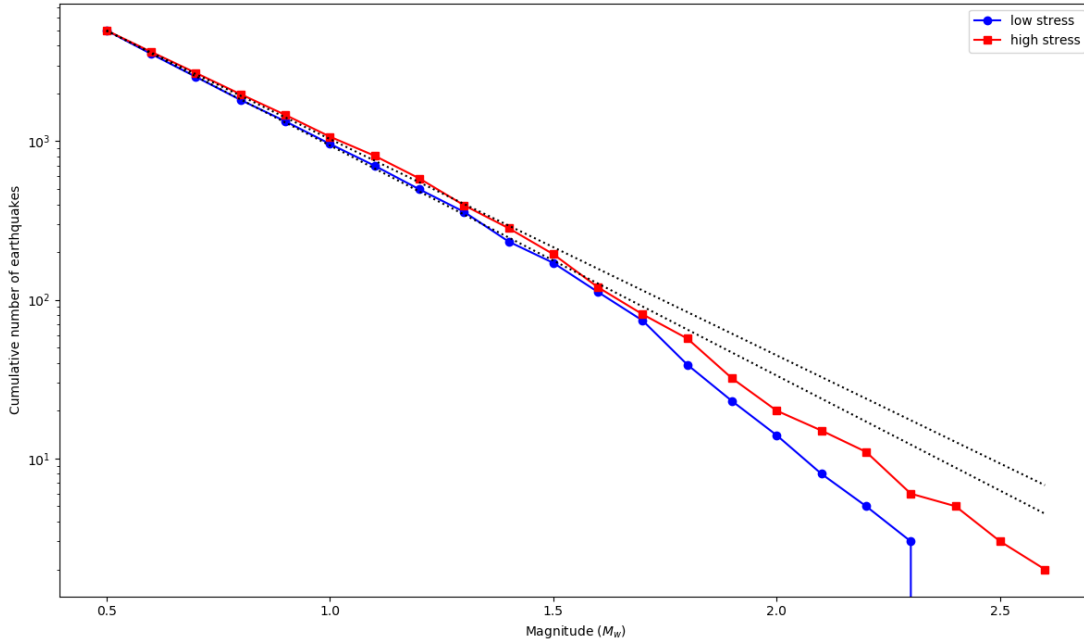


Figure 4. Cumulative FMDs of two groups of earthquakes, assuming $M_c = 0.5$: 5,000 earthquakes occurring during times of largest tidal stresses and 5,000 earthquakes occurring during times of smallest tidal stresses. The slope of the FMD of the low tidal stress group is consistently steeper (larger b value) than that of the high tidal stress group. Dotted lines indicate maximum likelihood fits to the data. The low tidal stress group has a b value of 1.451 ± 0.020 while the high tidal stress group has a b value of 1.358 ± 0.018 .

ure strength [Scholz, 1968]. Therefore, our observation of b value variation that is sensitive to small stress perturbations ($\sim 10^4$ more sensitive compared to previous observations [Scholz, 2015]) might be indicative of a very weak fault zone, consistent with observations of strong tidal triggering of earthquakes at Axial Seamount (Fig. S2) and other mid-ocean ridges [Wilcock *et al.*, 2016; Tolstoy *et al.*, 2002; Wilcock, 2001; Stroup *et al.*, 2007; Tan *et al.*, 2018]. This might also be due to having predominantly shallow earthquakes at < 2 -km depth with lower confining pressure, which means that tidal stresses may have a proportionately greater influence. The earthquakes could also primarily be crack-opening events, as rocks are known to have extremely low tensile strength. Finally, the tidal loading might have been significantly amplified due to the presence of a compressible magma reservoir [Albino *et al.*, 2010].

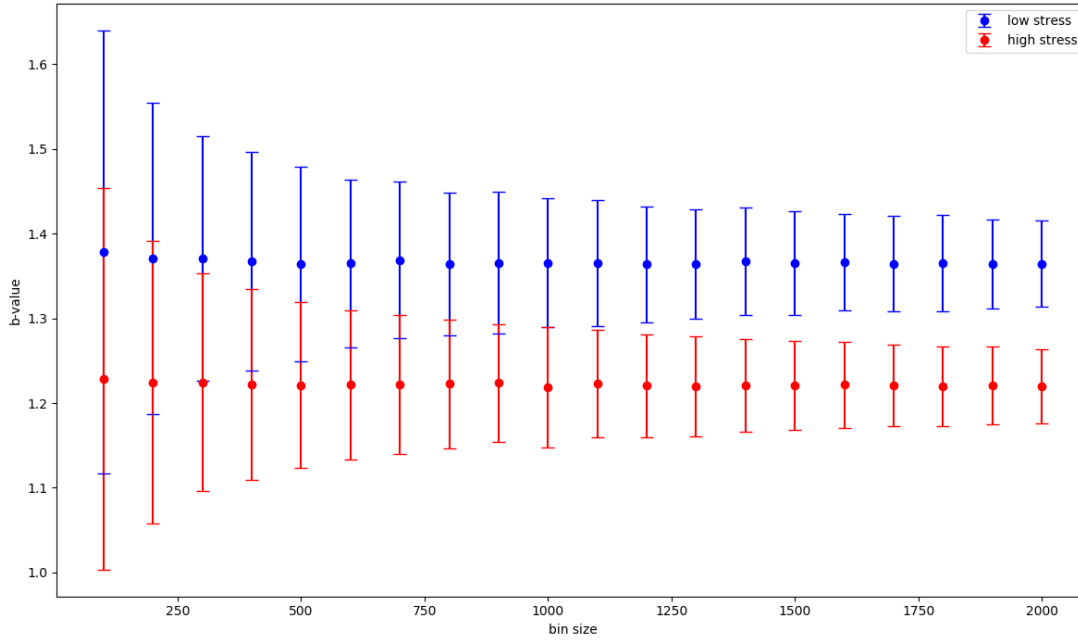


Figure 5. The estimated earthquake b values as a function of bin sizes. For each bin size, we calculate 1,000 b values using events randomly drawn without replacement from the original population. The vertical error bars represent two standard deviations. Events are drawn from two populations of earthquakes: 10,000 earthquakes occurring during times of largest tidal stresses and 10,000 earthquakes occurring during times of smallest tidal stresses (see Fig. 3)

4 Discussion and Conclusions

Our observed stress dependence of earthquake b values can be understood within the same statistical model first proposed to explain why the b values of microfractures in laboratory experiments vary with stress [Scholz, 1968]. If we treat the Earth’s crust as an inhomogeneous elastic medium experiencing a uniform applied stress, the presence of inhomogeneities means that the stress at each point within the crust is a random variable that follows a probability distribution function that depends on the uniform applied stress. If we further assume that at each point, fracture will occur if the local stress exceeds a critical value and that fractures stop growing when they propagate into a region of lower stress, it follows that a fracture has a higher probability of growing larger when the applied stress is greater [Scholz, 1968]. This translates to a decrease in b value with increasing stress.

A recent study using global data hinted at a b value-tidal stress correlation, as earthquake b values were found to decrease with increasing tidal shear stress ranking, where an earthquake's ranking is based on the maximum tidal shear stress during the day before the earthquake relative to the daily maxima in the 15 days before the earthquake *Ide et al.* [2016]. However, the relationship was not clear for earthquakes of $M_W < 6.5$ when looking at the Global Centroid Moment Tensor catalogue, potentially due to aggregating events of various faulting styles in diverse tectonic regimes [*Ide et al.*, 2016]. In addition, it is unclear why the earthquake b value would be sensitive to the tidal stress amplitude relative to the background daily maxima in the days before the event, instead of simply the absolute stress amplitude. Our natural experiment in a unique seafloor laboratory looking at the size distribution of earthquakes in a 25 km³ block of crust that experiences periodic tidal loading provides a robust test of the stress dependence of the earthquake b value. We find that the inverse relationship between b value and stress observed for small cracking events in laboratory experiments holds true for earthquakes in the natural environment, which increases the confidence in using earthquake b values to estimate spatial and temporal stress variations in the Earth's crust.

Acknowledgments

Y. J. T. thanks Göran Ekstrom, Meredith Nettles, Christopher Scholz, and Spahr Webb for fruitful discussions. This work was supported by NSF under grant OCE-1536320. The earthquake catalog used in this study is from *Wilcock et al.* [2016].

References

- Agnew, D. (1997), NLOADF: A program for computing ocean-tide loading, *J. Geophys. Res.*, *102*, 5109–5110.
- Aki, K. (1965), Maximum likelihood estimate of b in the formula $\log N = a - bM$ and its confidence limits, *Bull. Earthq. Res. Inst.*, *43*, 237–239.
- Albino, F., Pinel, V., and Sigmundsson, F. (2010), Influence of surface load variations on eruption likelihood: application to two Icelandic subglacial volcanoes, Grimsvotn and Katla, *Geophys. J. Int.*, *181*, 1510–1524.
- Amitrano, D. (2003), Brittle-ductile transition and associated seismicity: Experimental and numerical studies and relationship with the b value, *J. Geophys. Res.*, *108(B1)*, 2044, doi:10.1029/2001JB000680.

- Bohnenstiehl, D. R., M. Tolstoy, and F. Waldhauser (2008), Frequency-magnitude distribution of microearthquakes beneath the 9°50'N region of the East Pacific Rise, October 2003 through April 2004, *Geochem. Geophys. Geosyst.*, *9*(10), Q10T03, doi:10.1029/2008GC002128.
- Egbert, G. D., and S. Y. Erofeeva (2002), Efficient inverse modeling of barotropic ocean tides, *J. Atmos. Ocean. Tech.*, *19*, 183–204.
- Goebel, T. H. W., D. Schorlemmer, T. W. Becker, G. Dresen, and C. G. Sammis (2013), Acoustic emissions document stress changes over many seismic cycles in stick-slip experiments, *Geophys. Res. Lett.*, *40*, 2049–2054, doi:10.1002/grl.50507.
- Goebel, T. H. W., Kwiatek, G., Becker, T. W., Brodsky, E. E., and Dresen, G. (2017), What allows seismic events to grow big?: Insights from b-value and fault roughness analysis in laboratory stick-slip experiments, *Geology*, *45*, 815–818.
- Gulia, L., Tormann, T., Wiemer, S., Herrmann, M., and Seif, S. (2016), Short-term probabilistic earthquake risk assessment considering time-dependent b values, *Geophys. Res. Lett.*, *43*, 1,100–1,108.
- Gutenberg, B., and C. Richter (1944), Frequency of earthquake in California, *Bull. Seismol. Soc. Am.*, *34*, 185–188.
- Ide S., S. Yabe, and Y. Tanaka (2016), Earthquake potential revealed by tidal influence on earthquake size–frequency statistics, *Nat. Geosci.*, *9*, 834–837, doi:10.1038/NGEO2796.
- Levy, S. et al. (2018), Mechanics of fault reactivation before, during, and after the 2015 eruption of Axial Seamount, *Geology*, doi: <https://doi.org/10.1130/G39978.1>.
- Mignan, A., and J. Woessner (2012), Estimating the magnitude of completeness for earthquake catalogs, *Community Online Resource for Statistical Seismicity Analysis*, doi:10.5078/corssa-00180805.
- Mori, J. and Abercrombie, R. E. (1997), Depth dependence of earthquake frequency-magnitude distributions in California: Implications for rupture initiation, *J. Geophys. Res.*, *102*, 15,081–15,090.
- Nanjo, K. Z., Hirata, N., Obara, K., and Kasahara, K. (2012), ecade-scale decrease in b value prior to the M9-class 2011 Tohoku and 2004 Sumatra quakes, *Geophys. Res. Lett.*, *39*, L20304.
- Nishikawa, T., and S. Ide (2014), Earthquake size distribution in subduction zones linked to slab bouyancy, *Nat. Geosci.*, *7*, 904–908, doi:10.1038/NGEO2279.

- Savcenko, R. and W. Bosch (2012), EOT11a–Empirical ocean tide model from multi-mission satellite altimetry, *DGFI Report No. 89*.
- Scholz, C. H. (1968), The frequency-magnitude relation of microfracturing in rock and its relation to earthquakes, *Bull. Seismol. Soc. Am.*, *58*, 399–415.
- Scholz, C. H. (2015), On the stress dependence of the earthquake *b* value, *Geophys. Res. Lett.*, *42*, 1399–1402, doi:10.1002/2014GL062863.
- Schorlemmer, D., S. Wiemer, and M. Wyss (2005), Variations in earthquake-size distribution across different stress regimes, *Nature*, *437(7058)*, 539–542.
- Schorlemmer, D. and Wiemer, S. (2005), Microseismicity data forecast rupture area, *Nature*, *434*, 1,086.
- Shi, Y., and B. A. Bolt (1982), The standard error of the magnitude-frequency *b* value, *Bull. Seismol. Soc. Am.*, *72(5)*, 1677–1687.
- Spada, M., T. Tormann, S. Wiemer, and B. Enescu (2013), Generic dependence of the frequency-size distribution of earthquakes on depth and its relation to the strength profile of the crust, *Geophys. Res. Lett.*, *40*, 709–714, doi:10.1029/2012GL054198.
- Stroup, D. F., D. R. Bohnenstiehl, M. Tolstoy, F. Waldhauser, and R. T. Weekly (2007), Pulse of the seafloor: Tidal triggering of microearthquakes at 9°50'N East Pacific Rise, *Geophys. Res. Lett.*, *34*, L15301, doi:10.1029/2007GL030088.
- Stumpf, M., and M. Porter (2012), Critical truths about power laws, *Science*, *335(6069)*, 665–666.
- Tan, Y. J., M. Tolstoy, F. Waldhauser, and D. R. Bohnenstiehl (2018), Tidal triggering of microearthquakes over an eruption cycle at 9°50'N East Pacific Rise, *Geophys. Res. Lett.*, *45*, 1825–1831.
- Tolstoy, M., F. L. Vernon, J. A. Orcutt, and F. K. Wyatt (2002), Breathing of the seafloor: Tidal correlations of seismicity at Axial Volcano, *Geology*, *30*, 503–506.
- Tréhu, A. M., and S. C. Solomon (1983), Earthquakes in the Orozco Transform Zone: Seismicity, source mechanisms, and tectonics, *J. Geophys. Res.*, *88(B10)*, 8203–8225.
- Utsu, T. (1966), A statistical significance test of the difference in *b*-value between two earthquake groups, *J. Phys. Earth*, *14*, 34–40.
- Utsu, T. (1999), Representation and analysis of the earthquake size distribution: A historical review and some new approaches, *Pure Appl. Geophys.*, *155*, 509–535.
- Waldhauser, F., and W. L. Ellsworth (2000), A double-difference earthquake location and algorithm: Method and application to the northern Hayward Fault, California, *Bull. Seismol.*

- Soc. Am.*, 90, 1353–1368, doi:10.1785/0120000006.
- Wiemer, S., and K. Katsumata (1999), Spatial variability of seismicity parameters in aftershock zones, *J. Geophys. Res.*, 103, 13135–13151.
- Wiemer, S., and M. Wyss (2000), Minimum magnitude of completeness in earthquake catalogs: Examples from Alaska, the western United States, and Japan, *Bull. Seismol. Soc. Am.*, 90, 859–869, doi:10.1785/0119990114.
- Wilcock, W. S. D. (2001), Tidal triggering of microearthquakes on the Juan de Fuca Ridge, *Geophys. Res. Lett.*, 28, 3999–4002.
- Wilcock, W. S. D. et al. (2016), Seismic constraints on caldera dynamics from the 2015 Axial Seamount eruption, *Science*, 354(6318), 1395–1399.
- Wilcock, W. S. D. et al. (2018), The recent volcanic history of Axial Seamount: Geophysical insights into past eruption dynamics with an eye toward enhanced observations of future eruptions, *Oceanography*, 31(1), 114–123.

Supporting Information for

“Periodic tidal loading reveals stress dependence of the earthquake size distribution (b value)”

Yen Joe Tan¹, Felix Waldhauser¹, Maya Tolstoy¹, and William S. D. Wilcock²

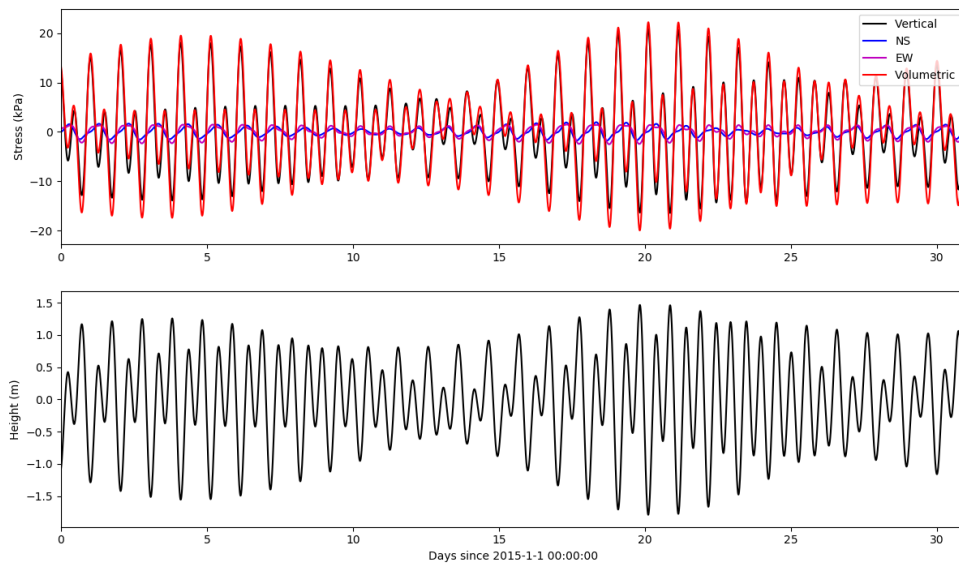
¹Lamont-Doherty Earth Observatory of Columbia University, Palisades, New York 10964, USA.

²School of Oceanography, University of Washington, Seattle, WA 98195, USA.

Contents

1. Figure S1

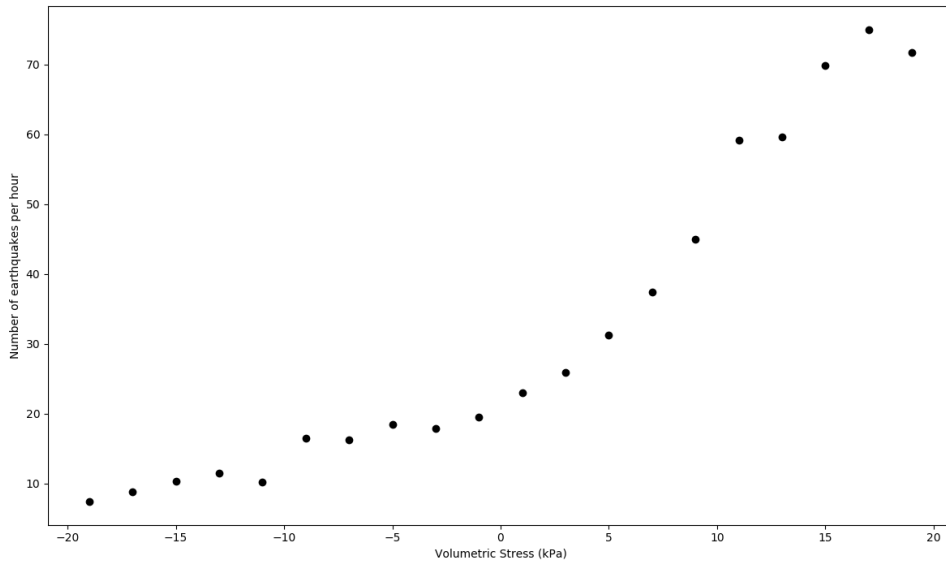
Time series of predicted tides at 45.95°N, 130.00°W. **a**, Estimate of vertical (black), N-S (blue), E-W (magenta), and volumetric (red) crustal stresses, with tensional stresses being positive. **b**, Predicted ocean tidal height.



2. Figure S2

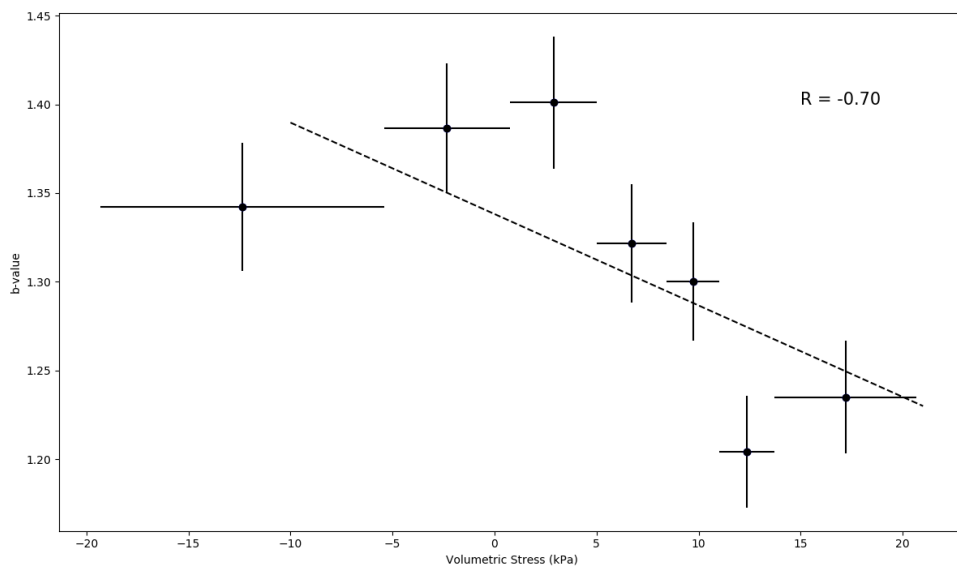
Seismicity rate as a function of tidal stress in non-overlapping stress bins of 2 kPa.

Corresponding author: Yen Joe Tan, yjt@ldeo.columbia.edu



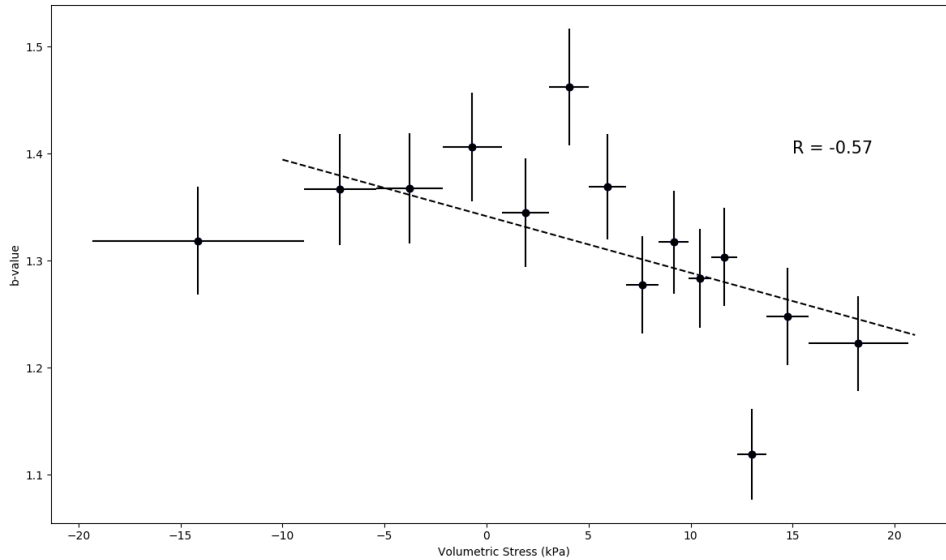
3. Figure S3

The earthquake b values as a function of tidal stress in non-overlapping bins of 5,000 earthquakes. The vertical error bars represent two standard deviations of the estimated b values. The horizontal bars represent the range of earthquake tidal stress values included in each bin. $b = 1.34 \pm 0.03 - (0.005 \pm 0.003)\sigma$ where stress is in kPa.



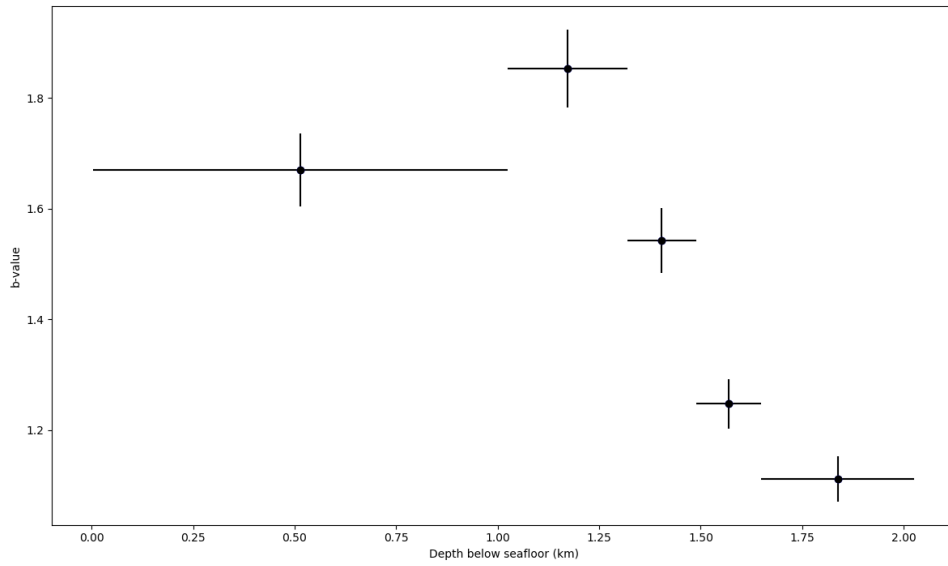
4. Figure S4

The earthquake b values as a function of tidal stress in non-overlapping bins of 2,500 earthquakes. The vertical error bars represent two standard deviations of the estimated b values. The horizontal bars represent the range of earthquake tidal stress values included in each bin. $b = 1.34 \pm 0.02 - (0.005 \pm 0.002)\sigma$ where stress is in kPa.



5. Figure S5

The earthquake b values as a function of depth in non-overlapping bins of 2,500 earthquakes. The vertical error bars represent two standard deviations of the estimated b values. The horizontal bars represent the range of earthquake depth values included in each bin. Since M_c is expected to vary with depth, we estimate M_c for different depth ranges before choosing a fixed $M_c = 0.4$ to estimate the b values.



6. Figure S6

The earthquake depth distribution in bins of 100 meters for (a) low tidal stress group and (b) high tidal stress group (see Fig. 3).

